Current Applied Science and Technology Vol. 23 No. 1 (January-February 2023)

Research article

Modeling a Simple Single-phase Grid-connected Photovoltaic System Using Negative Conductance of Solar Cells

Nuttakrit Somdock[1]*, Chatrpol Pakasiri[2], Aparpron Sakulkalavek[1] and Wichit Sirichote[1]

[1]*Department of Applied Physics, King Mongkut's Institute of Technology Ladkrabang, Ladkrabang, Bangkok, Thailand*
[2]*College of Advanced Manufacturing Innovation, King Mongkut's Institute of Technology Ladkrabang, Ladkrabang, Bangkok, Thailand*

Received: 2 January 2022, Revised: 9 April 2022, Accepted: 13 June 2022

DOI: 10.55003/cast.2022.01.23.009

Keywords

grid-connected photovoltaic system;

solar cell;

negative conductance;

simulations

Abstract

This paper presents the simulation of a simple single-phase grid-connected photovoltaic (PV) system using the PSPICE model. The modeling system consists of a PV string, a single-phase current source inverter (CSI), load, and a grid voltage source. The system uses the PV string as the current source. The single-phase CSI was controlled by the grid AC voltage. The operation of the system employs the negative conductance characteristics of the PV string. We studied the voltage and current waveform at the inverter output terminal, the current waveform at the load, the AC power with various open-circuit voltages and temperatures of the PV string. The result showed the current waveform at the inverter output terminal follows the I-V characteristics of the PV string. The current waveform at the load depends on its impedance characteristics. The AC power increased with the open circuit voltage. We found that the maximum efficiency of the AC power conversion system was 63.3% at the peak of the AC voltage source, which was equal to the maximum power voltage of the PV string. In addition, the prototype was built for testing and testing verified the simulation results. The experimental results showed the current waveform at the inverter terminal and load were similar to the simulation results.

1. Introduction

Solar energy is of importance in the reduction of the pollution effects of fossil-based energy systems, is sustainable and clean, and is pollution-free [1-3]. A solar cell or photovoltaic (PV) module is a semiconductor device that uses the photovoltaic effect to convert sunlight (solar energy) into electricity [4, 5]. The application of PV modules for PV systems is classified into two types: stand-

*Corresponding author: Tel.: (+66) 972528395 Fax: (+66) 3298412
E-mail: nuttakrit.so@kmitl.ac.th

alone PV and grid-connected PV systems [6, 7]. A stand-alone PV system of the DC type includes a PV string or PV array, a DC load, and battery storage. It can connect an AC load using a voltage regulator and a DC-AC inverter [8]. However, the cost of installation and maintenance are high, and the deterioration of the battery storage shortens its lifespan [9]. The main components of a grid-connected PV system are either a PV string or a PV array, an inverter, and the grid without battery storage. There are two main types of grid-connected PV systems: single-phase and three-phase grid-connected PV systems. The single-phase and three-phase grid-connected PV systems are connected to the grid via single-phase two wire and three-phase three wire systems, respectively [10]. There has been a lot of research concerned with single-phase grid-connected PV systems. Generally, a single-phase inverter uses either a standard full-bridge voltage source inverter (VSI) or a standard full-bridge CSI, depending on the nature of input power source [11]. Normally, the operation of a single-phase VSI and CSI inverter to control and create a sinusoidal voltage and current for injecting the current from the PV string to the grid is done by a microprocessor [12, 13]. A pulse width modulation (PWM) algorithm was used to control a single-phase VSI and a single-phase CSI. A high switching frequency that could reduce the value of the inductance, capacitance, and the output ripple voltage and current from the single-phase VSI and the single-phase CSI, respectively, was a requirement for controlling the system [14, 15]. However, the frequency is limited by switching loss and sampling frequency of the processor. A line-transformer is often used in the system between the conversion stage and the grid. It ensures galvanic isolation between the system and the grid. In addition, if the single-phase grid-connected PV system uses the transformer to increase the DC/AC converter output voltage level to meet the grid voltage level, the transformer will increase the size and cost of the system and reduce its efficiency [16, 17].

In this paper, we studied the modeling of a simple single-phase grid-connected photovoltaic system as shown in Figure 1. The system is a simple circuit without inductance, line frequency, and a microprocessor for controlling single-phase CSI, and there is no conversion step needed to inject the current from the PV string into the grid voltage source. The operation of the system employs the negative conduction characteristics of the PV string to convert solar power into a grid voltage source. Moreover, the PV string can generate current to be supplied into a load directly.

The paper is organized as follows. Section 2 describes the fundamental PSpice model for the solar cell that is used to build up the PV string. A single-phase CSI topology is described in Section 2.1, and a simple single-phase grid-connected PV system is described in Section 2.2. Section 2.3 is a description of the components of the simulation grid-connected PV system using the PSpice program. The simulation results are described and analyzed in Section 3, which shows the I-V characteristic of the PV string, voltage and current waveform output at the single-phase CSI terminal, the electrical power output of the single-phase CSI, the electrical signal of the AC load and finding the maximum efficiency power conversion system. In Section 3.1, details of our experimental prototype system consisting of PV string, single-phase CSI, load, and the grid are given, and the system performance is compared with the simulation results.

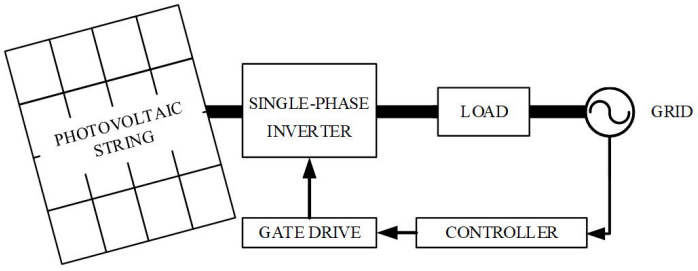

Figure 1. Block diagram of a single-phase grid-connected PV system

2. Materials and Methods

The solar cell is a p-n junction device that uses the PV effect to convert solar energy into electricity [18, 19]. When sunlight reaches a solar cell, it generates free carriers that flow through the load in a direct proportion to the intensity of incoming light at the p-n junction [20-22]. As illustrated in Figure 2, a simple equivalent circuit model of a solar cell was used in this research. The cell includes a current source, a diode, and two resistors [3, 23, 24].

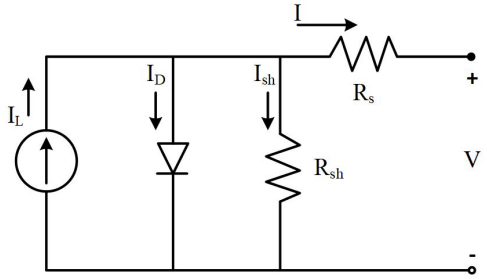

Figure 2. Equivalent circuit of a single solar cell

$$I = I_L - I_D - I_{sh} \tag{1}$$

Where I indicates the output current of the solar cell (A), the light-generated current in the solar cell is represented by I_L (A), the voltage-dependent current lost to recombination is represented by I_D (A), I_{sh} is the current lost due to shunt resistance (A). Equations 2 and 3 show the current of the diode I_D and the value of the shunt resistance R_{sh}, respectively.

$$I_D = I_0\left[\exp\left(\frac{V + IR_s}{nV_T}\right)\right] - 1 \tag{2}$$

$$I_{sh} = \frac{V + IR_s}{R_{sh}} \tag{3}$$

Where I_0 indicates the saturation current (A), the output voltage at the terminals is represented by V (V), the resistance is represented by R_s (Ω), the diode ideality factor is represented by n, the thermal voltage is represented by V_T (V). Substituting (2) and (3) into (1), equation 4 demonstrates the I-V characteristics of current and voltage in a single solar cell.

$$I = I_L - I_0\left(e^{\frac{V+IR_s}{nV_T}} - 1\right) - \frac{V + IR_s}{R_{sh}} \tag{4}$$

If we assume R_{sh} = infinity, when the solar produces no output current, the relationship between current and voltage at the solar cell terminals (V_{oc}) is simplified into equation 5.

$$I_0 = \frac{I_{sc}}{\left(e^{\frac{V_{oc}}{nV_T}} - 1\right)} \tag{5}$$

The I-V characteristics of a solar cell under light and dark conditions are shown in Figures 3(a) and 3(b), respectively. In the light condition, the difference between the voltage and the current is 180 degrees because the solar cell has a negative conductance [25]. The I-V characteristics of the solar cell is illustrated on the voltage axis in Figure 3(b). Note that at $V=V_{mp}$, the solar cell produces a maximum voltage. As the solar cell voltage V increases, its output current decreases. At $V=V_{oc}$, the solar cell is not generating current.

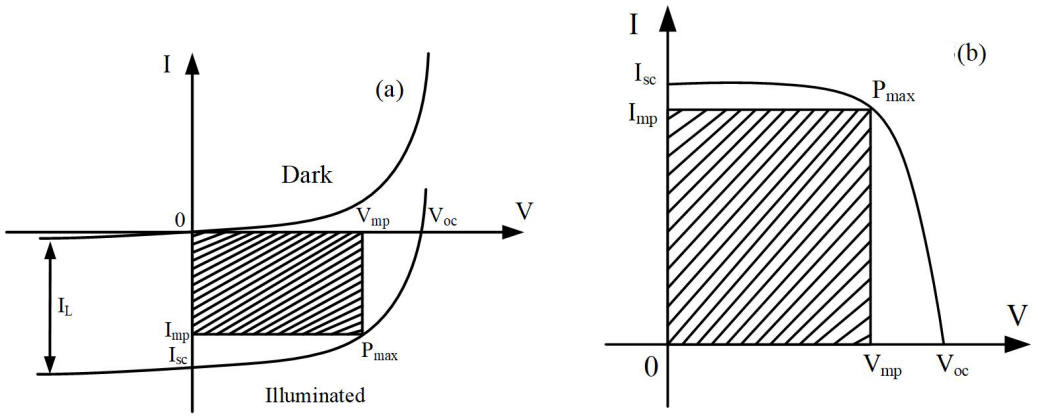

Figure 3. (a) I-V curve characteristics of solar cell under light and dark conditions; (b) inversion of (a) in the voltage axis

Generally, a PV module is formed by connecting solar cells in both series and parallel to increase the voltage and current output. A PV module grid is made up of solar cells connected by $N_s \times N_p$ elements, where the number of solar cells in a row is represented by N_s and the number of solar cells in a column is represented by N_p as shown in Figure 4. The following is a compact representation of the relationships between voltage and current in a PV module:

$$I_M = N_P I \tag{6}$$

$$I_{scM} = N_p I_{sc} \tag{7}$$

$$V_M = N_s V \tag{8}$$

$$V_{ocM} = N_s V_{oc} \tag{9}$$

$$R_{sM} = \frac{N_s}{N_p} R_s \tag{10}$$

Assuming R_{sh} = infinity, substituting equations (6)-(10) into equation (4) yields the output current of a PV module (I_M).

$$I_M = I_{scM}\left(1 - e^{\frac{V_M + I_M R_{sM} - V_{ocM}}{nV_T N_s}}\right) \tag{11}$$

Where I_{scM} indicates the short circuit current of a PV module (A), the voltage across a PV module is represented by V_m (V), the series resistance of a PV module is represented by R_{sM} (Ω), the open voltage circuit of the PV module is represented by V_{ocM} (V), and the thermal voltage is represented by V_T (V). The PV modules connected in series are called a PV string. The output current of a PV string is DC current [26].

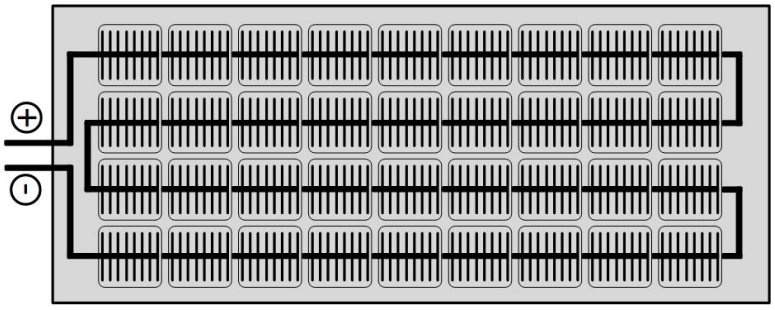

Figure 4. PV module

Nomenclature

DC	direct current	N_s	number of solar cells connected in series
AC	alternative current	N_p	number of solar cells connected in parallel
PV	photovoltaic	I_M	output current of a PV module
CSI	current source inverter	I_{scM}	PV module short-circuit current
VSI	voltage source inverter	V_M	voltage across a PV module
PWM	pulse width modulation	R_{sM}	series resistance of a PV module
I	solar cell output current	V_{ocM}	open voltage circuit of the PV module
I_L	light-generated current in the solar cell	I_{mp}	current at maximum power
I_D	voltage-dependent current lost to recombination	$P_{\max}$	power maximum of the either the PV module or the PV string
I_{sh}	current lost due to shunt resistance	IGBTs	Insulated Gate Bipolar Transistor
R_{sh}	shunt resistance	BJT	Bipolar Junction Transistor
I_0	saturation current	SCR	Silicon-Controlled-Rectifier
V	voltage across the output terminals	KVL	Kirchhoff's voltage law

R_s	series resistance	KCL	Kirchhoff's current law
n	diode ideality factor	V_{in}	DC power supply
V_T	thermal voltage	V_{load}	DC power at the load
V_{oc}	voltage at terminal of solar cell	$Load$	AC load line
V_{mp}	voltage at maximum power	I_{Load}	total current equaling to the sum of the currents in the branches
Q1-Q4	switching devices	I_{in}	current from DC power supply
$I_{PV\ string}$	current of PV string	$I_{current\ sourc}$	current from current source
$V_{PV\ string}$	voltage of PV string	I_{out}	current from the single-phase CSI
$v(t)_{load}$	voltage at the load	R	load resistance
V_p	peak voltage	S1-S4	gate controller
ω	angular speed expressed in radians per second	$v_g(t)$	AC source
θ	phase of the sinusoid expressed in degrees	$I_g(t)$	current from the AC source
t	time expressed in second	Vpulse	voltage Pulse Source Model
$+V_{in}$	voltage signal in the positive cycle	P_{AC}	AC power at output of the single-phase CSI
$-V_{in}$	voltage signal in the negative cycle	P_{DC}	DC power at input of the single-phase CSI
STC	standard condition of the PV module (temperature of 25°C and irradiance of 1000 W/m^2)		

2.1 Single phase inverter

Typically, a single-phase grid-connected PV system can change DC power into AC power using an inverter [27-29]. In this paper, we use a single-phase CSI, which is shown in Figure 5, to convert DC to AC power. The single-phase CSI is an electric device that changes DC power into AC power using a switching technique. A single-phase SCI consists of four-switching devices (Q1-Q4), which may be an Insulated Gate Bipolar Transistor (IGBT), a Bipolar Junction Transistor (BJT), a Silicon-Controlled-Rectifier (SCR) or any other similar switching device that can be operated electrically by applying a signal to the device's gate terminal [30]. The switching device can be operated in three stages: positive state, negative state and zero-potential voltage stages [27]. For each stage, a single-phase CSI produces a current across the load and the grid, as shown in Table 1. In Figure 5, diodes are added for safety reasons, e.g., to guard against short-circuiting if current from the PV string flows in the wrong direction when the single-phase CSI circuit malfunctions.

2.2 Principles of a single-phase grid-connected PV system

Usually, a single-phase grid-connected PV system is an auxiliary power system. It is therefore used with other power system. To simplify the system, we first considered a system shown in Figure 6. The DC power supply is the main system and the current source is the auxiliary power system. The load is connected to the main system and the auxiliary power system in order to use the power source. In the auxiliary system, the diode is connected in series with the current source to prevent the flow of electricity from the DC power supply into it.

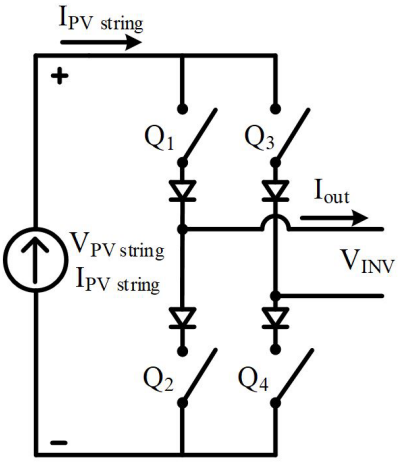

Figure 5. Single-phase CSI

Table 1. Switching stage single-phase CSI

Q1	Q2	Q3	Q4	Current across the load and the grid
On	Off	Off	On	Positive
Off	On	On	Off	Negative
On	On	Off	Off	Zero Potential
Off	Off	On	On	Zero potential

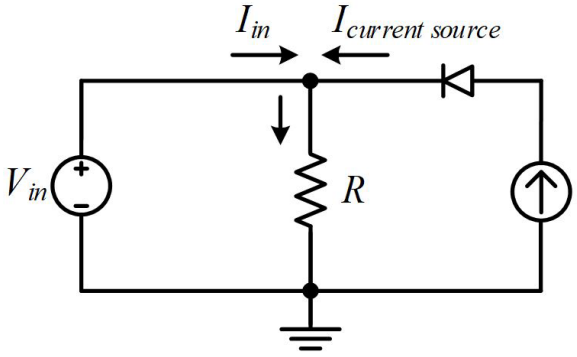

Figure 6. DC power supply connects to a DC load and a current source in parallel

Applying Ohm's law and Kirchhoff's voltage law (KVL), the load voltage and current can be found as:

$$V_{load} = (I_{in} + I_{current\ source})(R) \tag{12}$$

$$I_{load} = I_{in} + I_{current\ source} \tag{13}$$

Where V_{in} represents a DC power supply (V), V_{load} represents a DC power at the load, I_{load} represents the total current equaling to the sum of the currents in the branches (A), I_{in} is the current from DC power supply (A), $I_{current\ source}$ is the current from current source (A), and R is the load resistance.

A similar idea is applied to the PV string and the single-phase grid voltage source of 220Vrms 50Hz. A single-phase CSI is added to turn on/off electric current from PV string to the grid. The single-phase CSI was controlled by the AC power source. In addition, the diodes in the single-phase CSI help prevent current flow from the grid to the single-phase CSI and the PV string. The operation of single-phase grid-connected PV system uses the negative conductance characteristic of the PV string so that the electric current can flow into the grid. The equivalent circuit is shown in Figure 7.

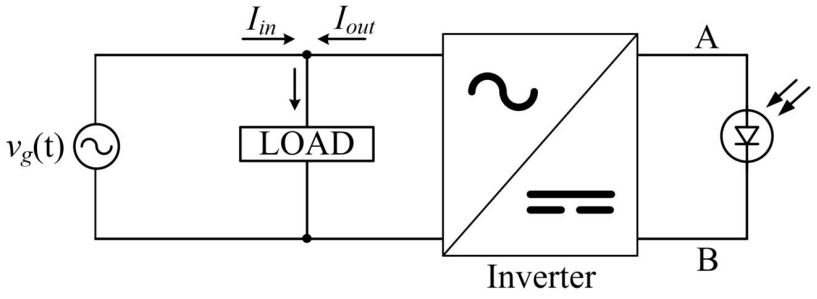

Figure 7. Equivalent circuit single-phase grid-connected PV system

The load can be found by applying Ohm's law and Kirchhoff's current law (KCL) and KVL as:

$$v(t)_{load} = (I_{in} + I_{out})(Load) \tag{14}$$

Where $v_g(t)$ represents an AC source, $v(t)_{load} = V_p \sin(\omega t + \theta)$ represents the voltage at the load (V), I_{in} is the current from AC power source (A), I_{out} is the current from the PV string (A), *Load* can be the AC load line. The current from the single-phase CSI, I_{out}, can be calculated as:

$$I_{out} = I_{scM}\left(1 - e^{\frac{v_g(t) + I_{out}R_{sM} - V_{ocM}}{nV_T N_s}}\right) \tag{15}$$

If the grid voltage is $v_g(t) = V_m \sin(\omega_t + \theta_v)$, the electrical current output of the single-phase CSI can be found as:

$$I_{out} = I_{scM}\left(1 - e^{\frac{V_p \sin(\omega t + \theta) + I_{out}R_{sM} - V_{ocM}}{nV_T N_s}}\right) \tag{16}$$

The output waveform of the grid voltage source and I-V curve characteristic from the PV string at standard condition (STC: temperature of 25°C and irradiance of 1000 W/m^2) are shown in Figure 8. If the peak of the grid voltage source is less than the PV string voltage at maximum power, the

system yields the low power. When the peak of the grid voltage source increases to peak voltage equal to 310V, the PV string reaches the PV string voltage at maximum power and therefore yields maximum power. However, if the voltage at maximum power of the PV string is greater than the peak of the grid voltage source, there will be the peak of the grid voltage was fixed which yields maximum power. To study the overall response of the single-phase grid-connected PV system by using negative conductance of the solar cells, the equivalent circuit model was simulated using PSpice program (PSpice 9.1 student version).

2.3 Analysis of the grid-connected photovoltaic system using PSpice program

Figure 9 shows the structure of a simple single-phase grid-connected PV system that consists of a PV string, single-phase CSI, grid voltage source and the load. The PV string uses mono-crystalline silicon PV SH80 modules. The specifications of the SH80 modules are summarized in Table 2. Figure 10 shows the I-V characteristics simulation results of SH80 modules for different values of irradiance. The load of the system consists of the 14.4 Ω resistor and 0.005 H inductor that are connected in parallel with the single-phase CSI and the grid voltage source of 220 Volt 50Hz.

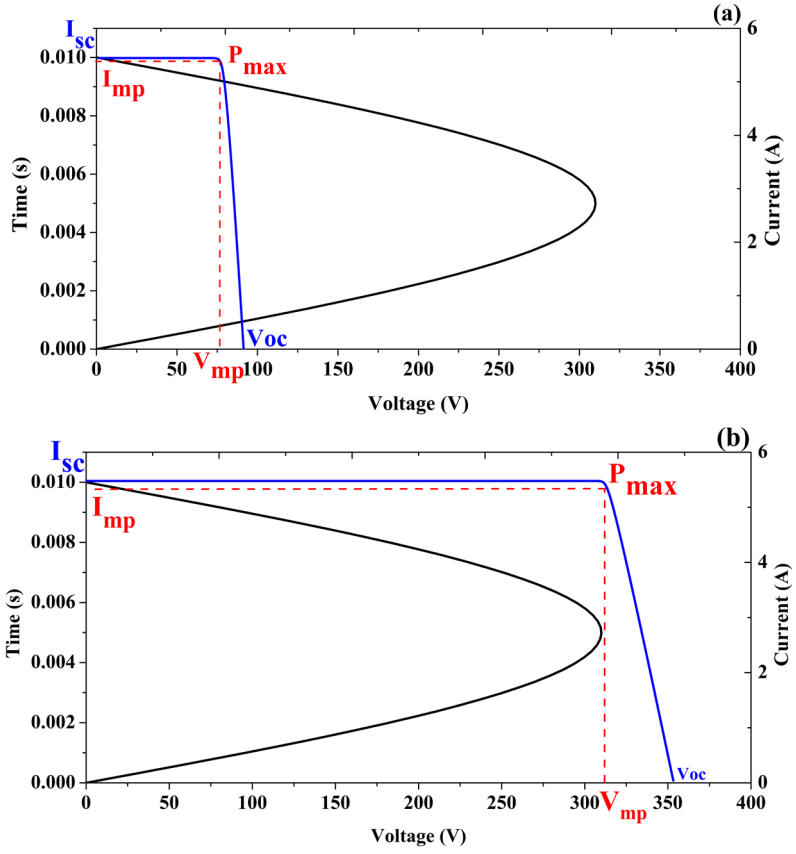

Figure 8. The relationships between output current and voltage of the PV string and the grid voltage source for (a) the peak of the grid voltage less than the PV string voltage at maximum power and (b) the peak of the grid voltage source greater than the PV string voltage at maximum power

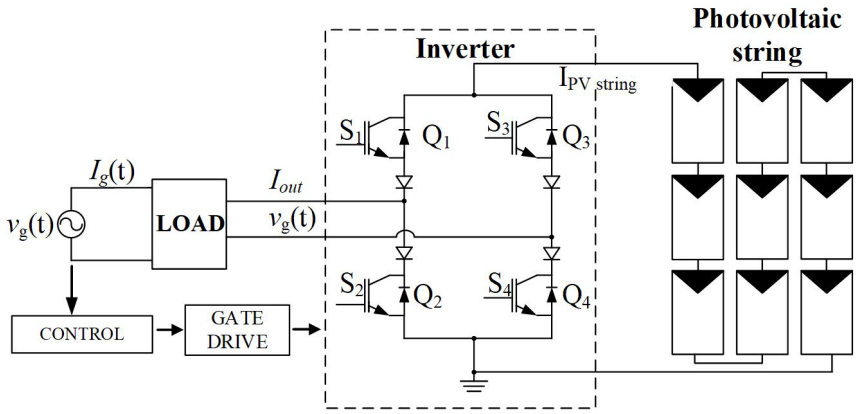

Figure 9. Proposed simple single-phase grid-connected PV system

Table 2. Specifications of mono-crystalline silicon PV modules at STC

Parameter	Sunhappy SH80
V_{oc}	21.8V
I_{sc}	4.96A
V_{mp}	17.6V
I_{mp}	4.55A
P_{max}	80W
N_s	36
N_p	1

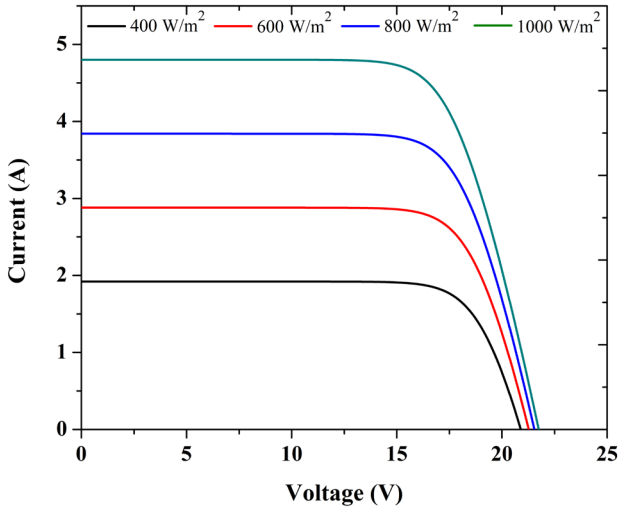

Figure 10. I-V characteristic simulation result of SH80 modules at various irradiance for a temperature of 25°C

Figure 9 shows a single- phase CSI circuit used for switching the current from the PV string into the load and the grid voltage source. The simulation consists of 4 switching devices Q_1, Q_2, Q_3 and Q_4, which are the IGBTs no. IRGPC30UD2. To control the switching operation of the IGBTs, control signals and voltage pulse source (Vpulse) are applied at their gates (S_1-S_4). For a single-phase CSI circuit with a gate controller, Vpulse (S_1-S_4) were used to control the switching device while four power diodes (D_1-D_4) no. 1N3891 were included for safety in case the current from the PV string flows in the wrong direction causing malfunction. For the operation modes of the single-phase CSI, there are two switching modes by which the gate controller controls the switch so that electricity for the PV string flows into the load and the grid. In the first operating mode, when the grid voltage source produces voltage signal in the positive cycle ($+V_{in}$), the switches Q_1 and Q_4 are turned on and the switches Q_2 and Q_3 are turned off. The current flows out of the PV string into the single-phase CSI through the switch Q_1. Then the current flows out of the single-phase CSI to the load and the grid producing positive voltage at the load and the grid voltage source, $+V_{in}$. After that, the current returns to the single-phase CSI through the switch Q_4. In the second mode, the grid voltage source produces voltage signal in the negative cycle ($-V_{in}$) and thus the switches Q_2 and Q_3 are turned on, but the switches Q_1 and Q_4 are turned off. The current flows out of the PV string into the single-phase CSI through the switch Q_3. Then the current flows out of the single-phase CSI to the load and the grid voltage source producing negative voltage at the load and the grid voltage source, $-V_{in}$. In the return path, the current flows out of the load and the grid voltage source to the single-phase CSI through the switch Q_2. The operation of the single-phase CSI is shown in Table 3.

Table 3. The operation of the single-phase CSI

The grid voltage source	**Vpulse**			
	S_1	**S_2**	**S_3**	**S_4**
$+V_{in}$	ON	OFF	OFF	ON
$-V_{in}$	OFF	ON	ON	OFF
0	OFF	OFF	On	On
0	On	On	Off	off

Figure 11 shows the waveform of the grid voltage source and the Vpulse signal to control the gate controller. These two signal sources are used in PSpice simulation. The results of the simulation are discussed in the next section

3. Results and Discussion

3.1 Simulation results

The simulation results are run at the PV string operating in the STC. The PV string used in the simulation study are from 4 PV modules to 18 PV modules yielding the open circuit voltage of the PV string from 67.1 to 420.7 V, respectively. The grid voltage source is fixed at 220 Vrms, 50 Hz. The simulation results of the simple single-phase grid-connected PV system are shown in Figures 12-14. In these figure, part (a) shows the I-V characteristics simulation results of the mono-crystalline silicon PV modules while part (b) shows the current and voltage waveform at the single-phase CSI terminal.

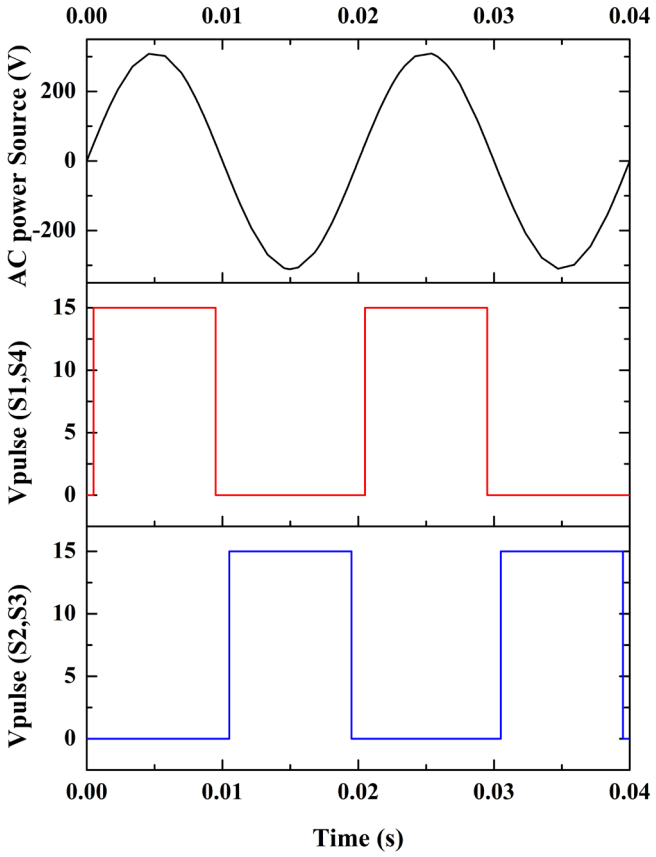

Figure 11. The grid voltage source signal and the gate control signal

First consider 4 PV modules in Figure 12. As the grid voltage source in Figure 12(b) starts from O to S, all the switches of the single-phase CSI are open so that there is enough time for both switch pairs not turning on at the same time. In Figure 12(b), the switches S1 and S4 of the single-phase CSI are turned on so that the current can flow out of the PV modules to the load and the grid voltage source from point S to A. As the grid voltage source approaches open circuit voltage of the 4 PV module (67.1 V), the current decreases according to the I-V characteristics curve shown in Figure 12(a). For the grid voltage source greater than the open circuit voltage, A to A' in Figure 12(b), the output current from the single-phase CSI becomes zero. As the grid voltage source decreases below open circuit voltage, A' to S' in Figure 12(b), the current out of the single-phase CSI can flow into the load and the grid voltage source. Then the switches S1 and S4 will be closed over the period S' to O', yielding no current into the load and the grid voltage source. For the PV string of 5, 6, 7, and 8 PV modules, the operation are similar except the open circuit voltages are 113.5, 136.9, 160.4, and 184.1 V, respectively. A similar operation occurs for the negative grid voltage cycle. For the PV string of 5, 6, 7, and 8 PV modules, the operation are similar except the open circuit voltages are 113.5, 136.9, 160.4, and 184.1 V, respectively. Therefore, in Figure 12(b), the 8 PV modules yield the longest period of current flow to the load and the grid voltage source.

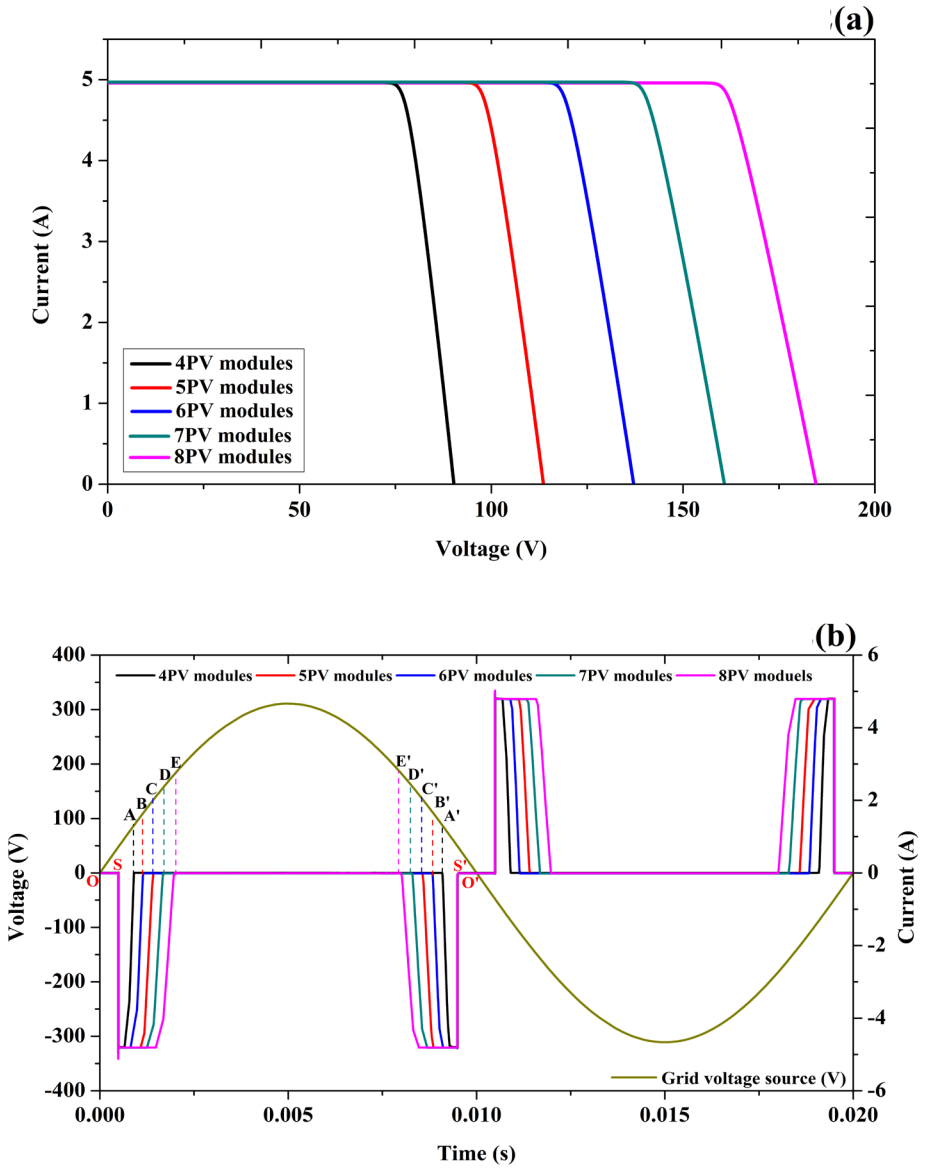

Figure 12. Simulation results of the grid-connected PV system with 4-8 PV modules; (a) The I-V characteristics simulation results of the mono-crystalline silicon PV modules, (b) The voltage input and the current output waveform of a single-phase CSI

Figure 13 shows the simulation results of the PV string of 9, 10, 11, 12 and 13 PV modules. Similar output voltage and current behaviors to those of Figure 12 are presented. The open circuit voltage for 9, 10, 11, 12 and 13 PV modules are 207.9, 231.9, 255.9, 279.9, and 323.3V, respectively. At this point, it is found that as the number of PV modules increases, the output current flowing period to the load and the grid voltage source increases.

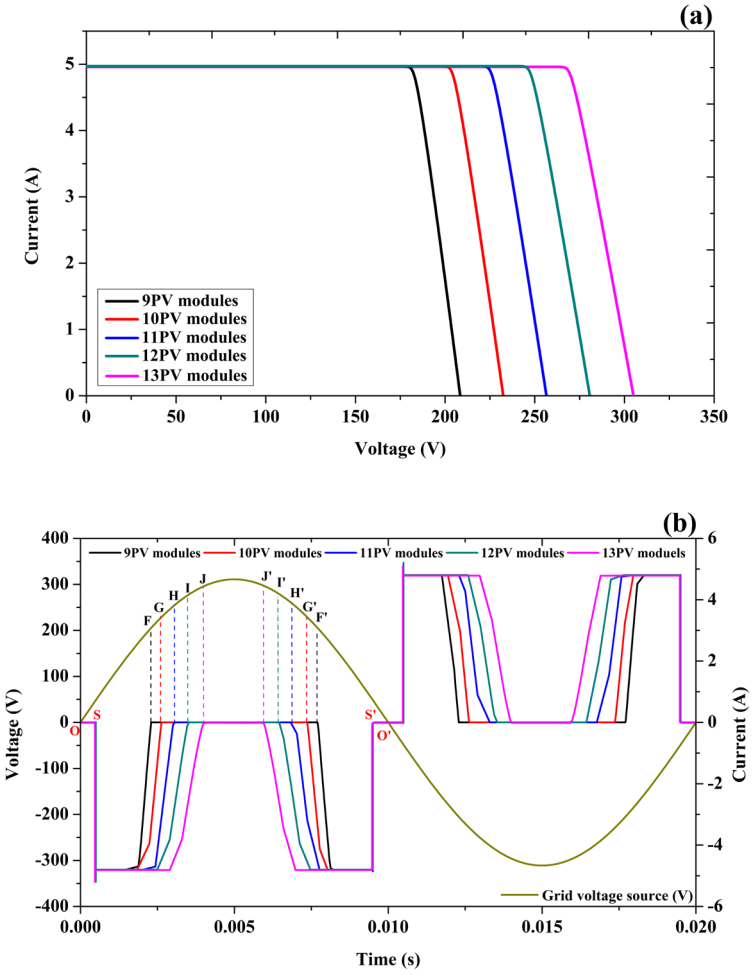

Figure 13. Simulation results of the simple single-phase grid-connected PV system with 9-13 PV modules; (a) The I-V characteristics simulation results of the mono-crystalline silicon PV modules, (b) The voltage input and the current output waveform of a single-phase CSI

Figure 14 shows the simulation results of the system with 14-18 PV modules. For these cases, the open circuit voltage of the PV string is greater than the peak of the grid voltage source. Therefore, there will always be current flowing out of the single-phase CSI as long as the switches are closed. If the open circuit voltage of the PV string is greater than the peak of the grid voltage source but less than the voltage at maximum power of the PV string, the current waveform will drop from the maximum value for some times. For example, considering the output current for the 14 and 15 PV modules as shown in Figure 14(b), the system yields low power. If the peak of the grid voltage is equal to the voltage at maximum power of the PV string, the system yields the maximum power from the system. However, if the voltage at maximum power of the PV string is greater than the peak of the grid voltage source, then the peak of the grid voltage is fixed, which yields maximum power. The voltage and current waveform output at the single-phase CSI terminal in Figures 12(b), 13(b), and 14(b) show negative conduction characteristics of the PV string in the grid voltage source.

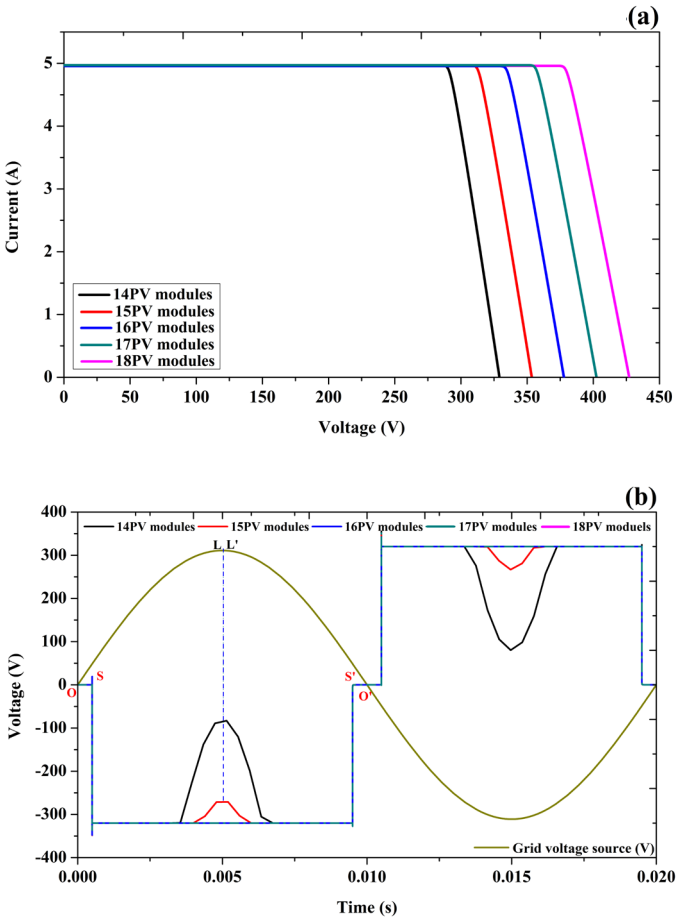

Figure 14. Simulation results of the grid-connected PV system with 14-18 PV modules; (a) The I-V characteristics simulation results of the mono-crystalline silicon PV modules, (b) The voltage input and the current output waveform of a single-phase CSI

Figure 15 shows simulation results of the output AC power single-phase CSI. At this load, the voltage and current waveform are smooth and sinusoidal, which proves that the simple single-phase CSI can generate current to be supplied into a load directly.

Figure 16 shows the efficiency of the implemented proposed simple single-phase grid-connected PV system. The DC power input assumes the maximum power of the PV string at the STC and the maximum efficiency of the AC power conversion system. The maximum power of the PV string increases as the number of the PV modules increases from 4PV to 15PV modules. The output AC power of the single-phase CSI also increases as the number of the PV module increases. The output AC power of the single-phase CSI reaches the maximum value when the number of the PV modules is 15 due to the peak of AC voltage source being equal to the maximum power voltage of the PV string. Moreover, adding more PV modules decreases the efficiency of the AC power conversion system because the output DC power from the photovoltaic string keeps increasing while the value of the AC power output at the single-phase CSI output terminal does not change.

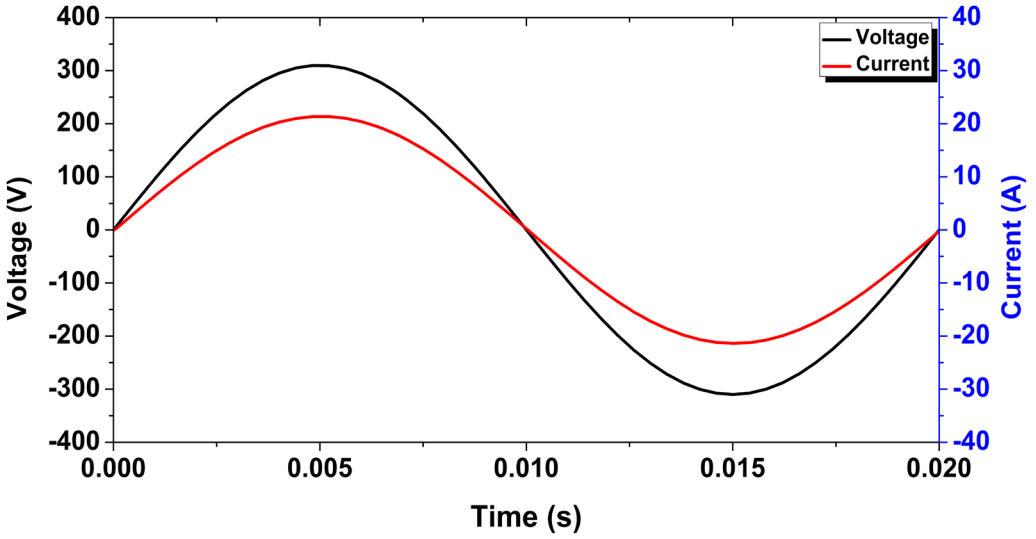

Figure 15. Simulation results of the output voltage and current waveforms at the load

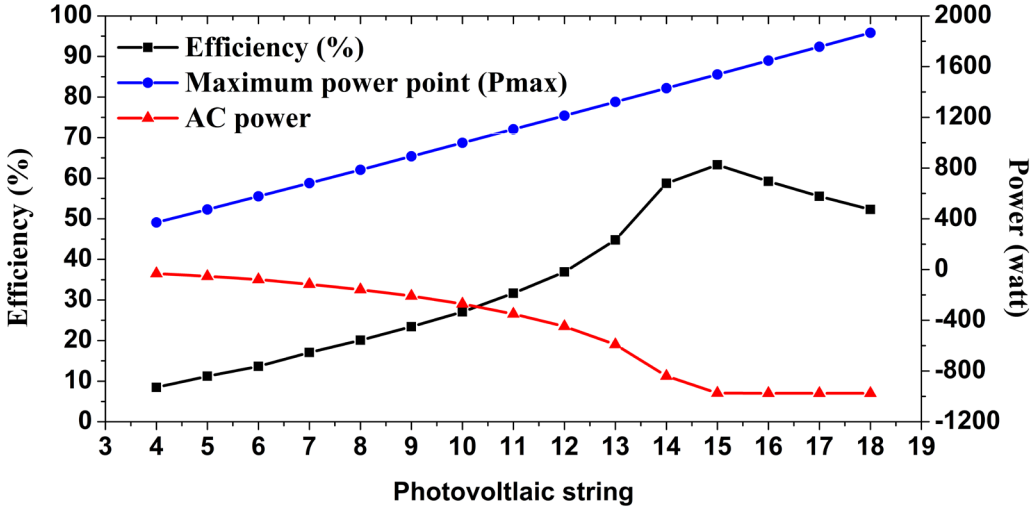

Figure 16. Efficiency, maximum power of the PV string and AC power output at single-phase CSI at the STC

The efficiency of a solar inverter conversion system is calculated by

$$\eta_{inv} = P_{out} / P_{in} \tag{17}$$

and percentage of efficiency can be calculated from

$$\eta\% = P_{out} / P_{in} \times 100 \tag{18}$$

Where P_{out} represents the AC power output of the single-phase CSI, P_{in} is the DC power input of the single-phase CSI [31-35].

Figure 17 shows simulation results using 15 PV modules with various temperature values and fixed nominal solar irradiance of 1000 W/m^2. If the temperature of the PV string is increased from 15ºC to 25ºC, the maximum power of the PV string increases while the output AC power magnitude also increases. If the temperature of the PV string is increased from 40ºC to 60ºC, the maximum power decreases while the output AC power magnitude also decreases. The efficiency of the system at 15, 25, 40, and 60ºC were 61.47, 63.30, 61.93, and 53.70%, respectively.

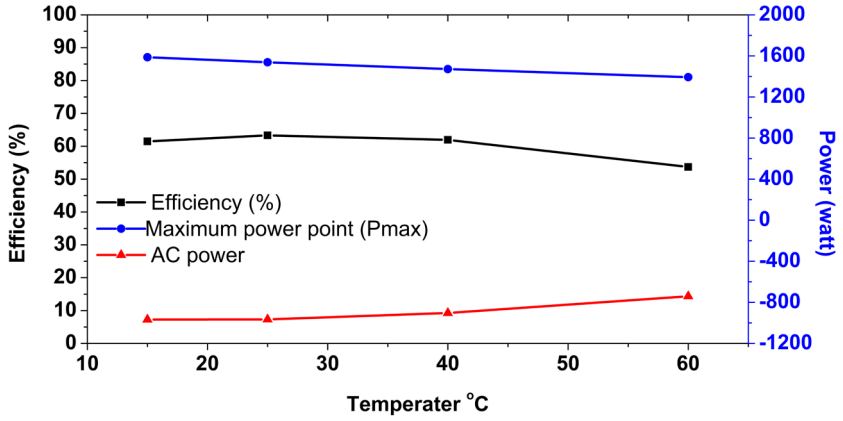

Figure 17. Simulation results using 15 PV modules with temperature values of 15, 25, 40, and 60ºC and a nominal solar irradiance of 1000 W/m^2

3.2 The experiment results

The schematic circuit of the simple single-phase grid-connected PV system is shown in Figures 18(a) and (b). The system consists of four G20N60B3D N-channel IGBTs, and four gate switches. The controller circuit part consists of an isolating transformer (220 V to 12 V) connected to an AC-pulse converter IC7667, used to control the gates of IGBTs and four power diodes number 25FR80 included for safety. The transformer is an isolation transformer using the primary coil and the secondary coil to step down AC source voltage connected to the IC7667 to control the gate switches. The system is connected to the grid voltage source of 220 Vrms 50 Hz in synchronous mode. Figure 18(c) shows a prototype of the simple single-phase grid-connected PV system. The PV string was tested with a variation of PV modules: 10, 15 and 20, respectively. Experimental results of the voltage and current waveforms at the single-phase CSI output terminal measured by power analyzer CA 8230 are shown in Figure 19.

From Figure 19, the voltage and current shows similar trends to those of the simulation. Nevertheless, measurement and simulation conditions are different in that the irradiance in the measurement may vary from the ideal value of 1000 W/m^2 and the measured temperature is different from 25ºC. The measurement data shows that the output power from the PV system is negative as expected, compared to the results from the simulation.

Figure 20(a) shows the voltage and current waveform output of the single-phase CSI terminal with 20 PV modules. However, the measurement was performed in an uncontrolled environment of the PV string in the STC, so the result did not show the maximum current output in the system. An incandescent lamp was used in the load that connected in parallel with the single-phase CSI terminal. Figure 20(b) shows the voltage and current waveforms of the load.

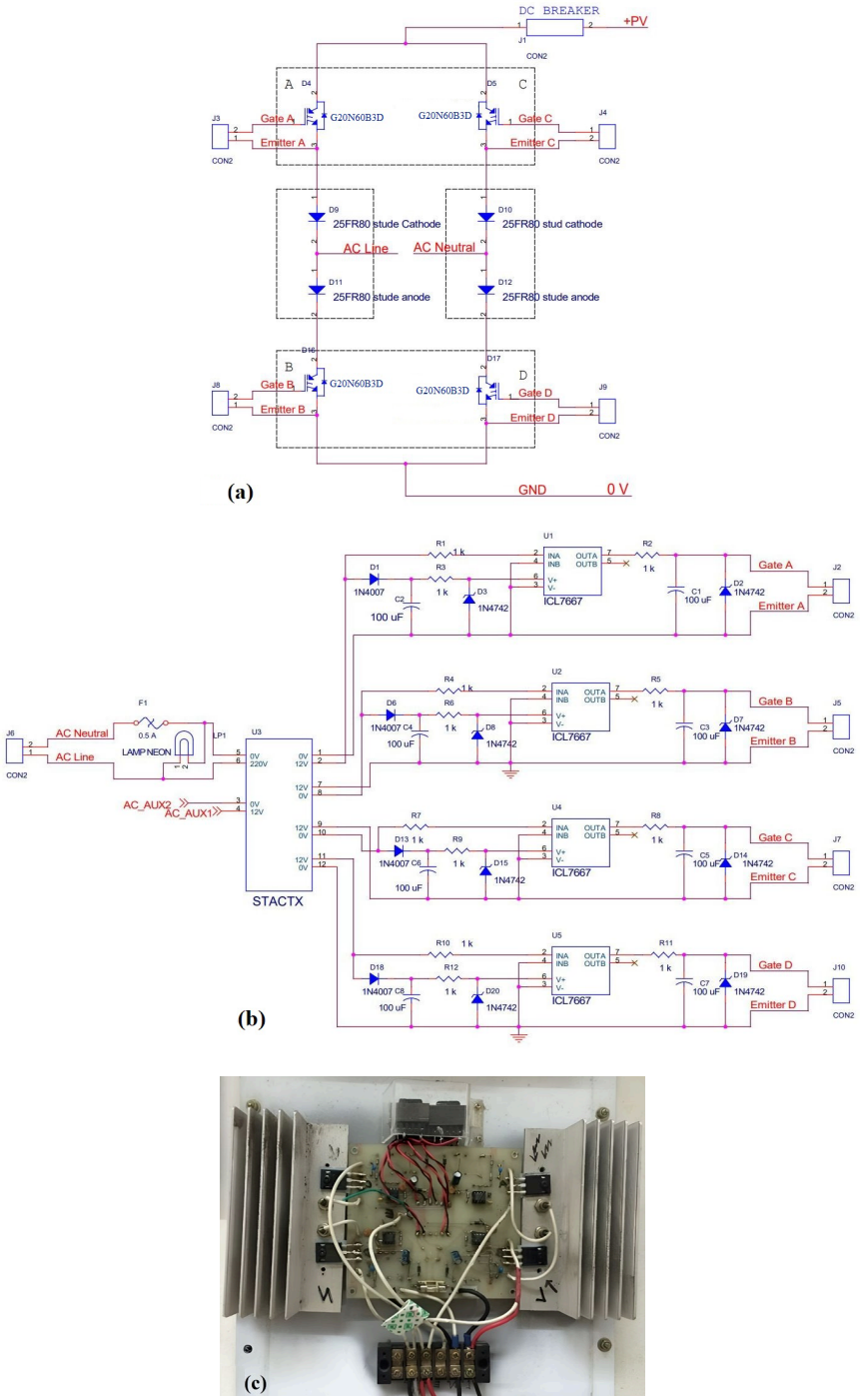

Figure 18. The schematic circuit of: (a) simple inverter single-phase CSI, (b) the control system of the simple inverter single-phase CIS (c) the prototype of the simple single-phase CSI system

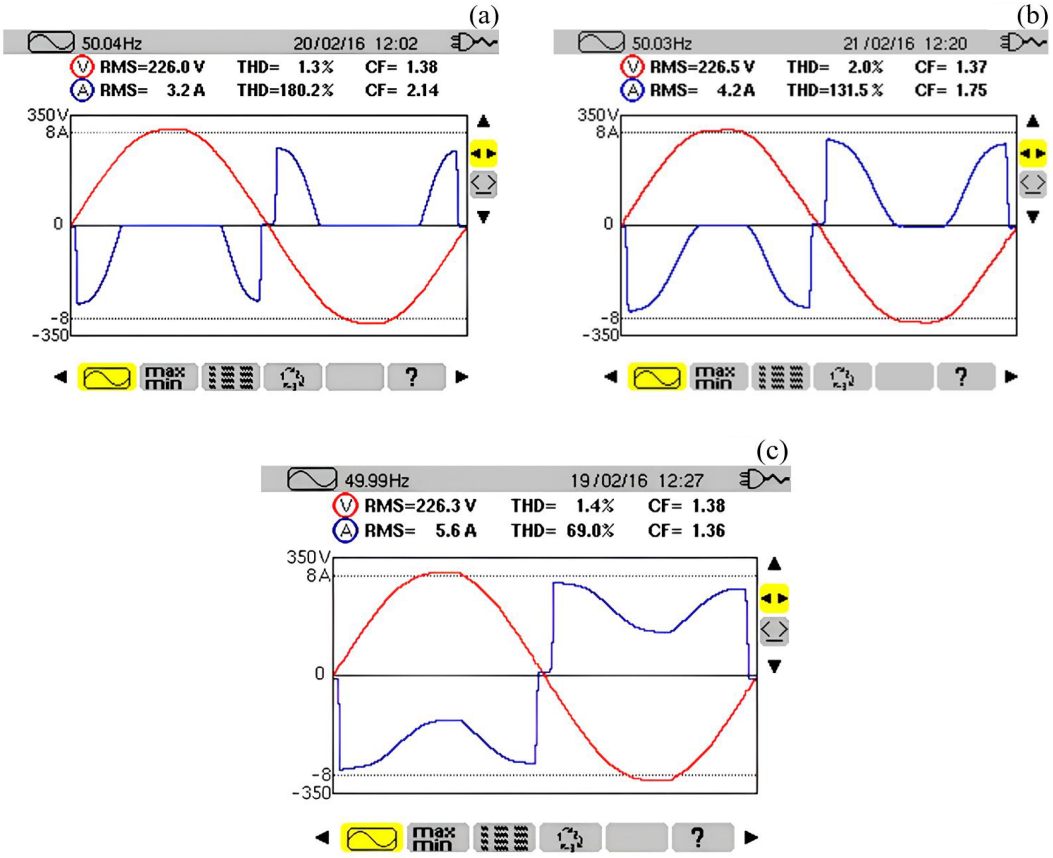

Figure 19. The voltage input and current output waveforms of the single-phase CSI (a) 10 PV modules, (b) 15 PV modules, and (c) 20 PV modules

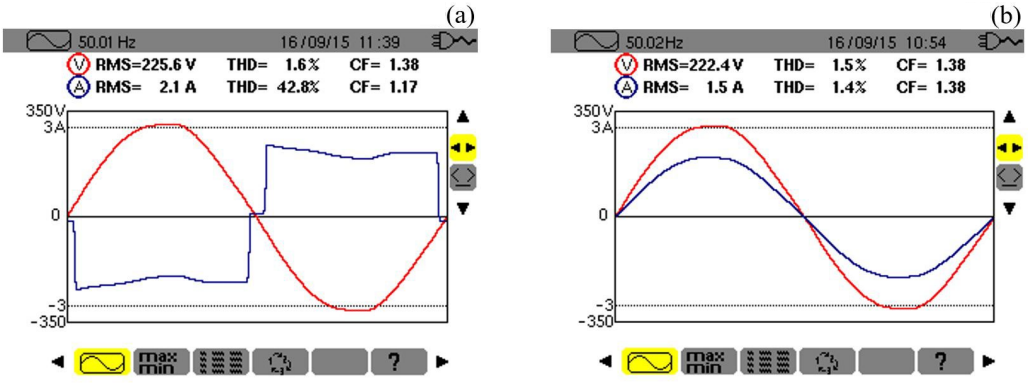

Figure 20. Experiment results of the simple single-phase grid-connected PV system with 20 PV string measured by power analyzer CA 8230, (a) Voltage and current waveforms output of the single-phase CSI terminal, (b) Voltage and current waveforms of the load

Consequently, the simple single-phase grid-connected PV system uses the negative conductance of solar cell that can convert solar power to the grid voltage source. The system does not use line-transformers, inductance and microprocessors to control single-phase CSI. The single-phase CSI was controlled by the AC power source. The simulation and the experimental results show the voltage and current waveform at the single-phase CSI terminal were 180 degrees opposite to each other. This behavior was in agreement with the literatures [12]. The output voltage waveform at the single-phase CSI terminal depends on the grid voltage source, and the output current waveform at the single-phase CSI terminal depends on the open circuit of the PV string and the voltage at maximum power of PV string. The maximum efficiency power conversion system of 63.3% occurred when the voltage at maximum power of the PV string equaled the peak grid voltage source. The system is a current source inverter, and the power quality is based on voltage quality [31]. Therefore, the current waveform at the load as well as its magnitude is based on the nature of load impedance [36].

4. Conclusions

The simulation of a simple single-phase grid-connected PV system was done using the PSPICE model. The modelling system was composed of a PV string, a single-phase CSI, load and the grid voltage source. The system uses the PV string as the current source. The single-phase CSI was controlled by the grid AC voltage. Once the single device parameters were defined, the simulation inputs were the load, the open-circuit voltage and the temperature of the PV string. The dynamics of the system were characterized using the model. It was used to evaluate the influence of solar irradiation intensity, solar cell temperature, the open-circuit voltage of the PV string and the behavior of the system. The content of the output waveform was used to study behavior with the negative conductance of the PV string in order to convert solar power into the grid voltage. The open-circuit voltage source of the PV string, solar irradiation intensity, solar cell temperature, the output waveform at the single-phase CSI, the output waveform at the load, the AC power output from the single-phase CSI and the efficiency of the AC power conversion system variations were evaluated.

This work showed the potential of the simulation of the system, which allowed us to obtain a deeper knowledge of the circuit performance. The use of the negative conductance of the PV string allowed us to obtain realistic simulation results. The simulation results showed that as the open circuit voltage of the PV string increased, the output AC power and the maximum power voltage of the PV string also increased. The maximum of AC power conversion system was 63.3%, which occurred at the peak of AC voltage source equal to the maximum power voltage of the PV string.

The proposed circuit prototype for the system was measured with various PV module numbers. The experimental results showed that the voltage and the current waveform changed as the open-circuit voltage of the PV string increased. The measured data is consistent with the simulation results. The proposed system offers a simple and promising way to convert power from the PV system to a desired load and to connect to the grid voltage source.

References

[1] Tawalbeh, M., Al-Othman, A., Kafah, F., Abdelsalam, E., Almonani, F. and Alkasrawi, M., 2021. Environmental impacts of solar photovoltaic systems: A critical review of recent progress and future outlook. *Science of The Total Environment*, 759, DOI: 10.1016/j.scitot env.2020.143528.

[2] Rafał, B., Błachut, J., Ciepiela, A. and Łabuz, R., 2021. Renewable energy sources vs. an air quality improvement in urbanized areas - the metropolitan area of Kraków case. *Frontiers in Energy Research*, 9, DOI: 10.3389/fenrg.2021.767418.

[3] Sirichote, W., Wuttikornkanarak, C., Srathongkao, S., Suttiyan, S., Somdock, N. and Klongratog, B., 2021. IV tracer for photovoltaic panel. *Proceedings of the 7th International Conference on Engineering, Applied Sciences and Technology (ICEAST)*, Pattaya, Thailand, April 1-3, 2021, pp. 54-57.

[4] Nwaigwe, K.N., Mutabilwa, P. and Dintwa, E., 2019. An overview of solar power (PV systems) integration into electricity grids. *Materials Science for Energy Technologies*, 2(3), 629-633.

[5] Adel, Y., Abdelhady, R. and Ibrahim, A.M., 2016. Assessment of a proposed hybrid photovoltaic array maximum power point tracking method. *Water Science*, 30(2) 108-119.

[6] Menaga, D. and Velupillai, D., 2021. Performance comparison for grid connected photovoltaic system using sliding mode control. *Journal of King Saud University - Engineering Sciences*, 33(4) 276-283.

[7] Sujatha, B.G. and Anitha, G.S., 2018. Enhancement of PQ in grid connected PV system using hybrid technique. *Ain Shams Engineering Journal*, 9(4), 869-881, DOI: 10.1016/j.asej.2016.04.007.

[8] Akash-Kumar, S., Kumarasamy, S. and Prashant, B., 2016. Design, simulation and economic analysis of standalone roof top solar PV system in India. *Solar Energy*, 136, 437-449.

[9] Narayan, N., Papakosta, T., Vega-Garita, V., Qin, Z., Popovic-Gerber, J., Bauer, P. and Zeman, M., 2018. Estimating battery lifetimes in solar home system design using a practical modelling methodology. *Applied Energy*, 228, 1629-1639.

[10] Kumar, N., Tapas-Kumar, S. and Dey, J., 2016. Modeling, control and analysis of cascaded inverter based grid-connected photovoltaic system. *International Journal of Electrical Power and Energy Systems*, 78, 165-173.

[11] Lakshika, K.A.H., Boralessa, M.A.K.S., Perera, M.K., Wadduwage, D.P., Saravanan, V. and Hemapala, K.T.M.U., 2020. Reconfigurable solar photovoltaic systems: A review. *Heliyon*, 6(11), DOI : 10.1016/j.heliyon.2020.e05530.

[12] Sang-Hun, L, Sung-Geun, S., Sung-jun, P., Chae-joo, M., and Man-Hyung, L., 2008. Grid-connected photovoltaic system using current-source inverter. *Solar Energy*, 82(5), 411-419.

[13] Abo-Elyousr, F.K. and Abdelaziz, A.Y., 2018. Optimal PI microcontroller-based realization for technical trends of single-stage single-phase grid-tied PV. *Engineering Science and Technology, an International Journal*, 21(5), 945-956, DOI: 10.1016/j.jestch.2018.07.007.

[14] Blaacha, J., Aboutni, R., Chennaif, M. and Aziz, A., 2021. Design of a single-phase inverter controlled by a digital PWM for the optimization of photovoltaic energy. *Materialstoday: Proceedings*, 45(8), 7774-7781.

[15] Bayhan, S., Trabelsi, M. and Abu-Rub, N., 2017. Model predictive control based current ripple damping in single-phase quasi-impedance-source inverter. *Proceedings of the 19th European Conference on Power Electronics and Applications (EPE'17 ECCE Europe)*, Warsaw, Poland, September 11-14, 2017, pp. 39-46.

[16] Ahmed-Zaid, S. and Kassem, A.M., 2017. Review, analysis and improving the utilization factor of a PV-grid connected system via HERIC transformerless approach. *Renewable and Sustainable Energy Reviews*, 73, 1061-1069.

[17] Ahmad, Z. and Singh, S.N. 2017. Comparative analysis of single phase transformerless inverter topologies for grid connected PV system. *Solar Energy*, 149, 245-271.

[18] Rezaee-Jordehi, A., 2016. Parameter estimation of solar photovoltaic (PV) cells: A review. *Renewable and Sustainable Energy Reviews*, 61, 354-371.

[19] Naahidi, S., Sama, N., Navid, M.S.J. and Sheva, N., 2020. Rise of nature-inspired solar photovoltaic energy convertors. *Solar Energy*, 208, 31-45.

[20] Tervo, E.J., Callahan, W.A., Toberer, E.S., Steiner, M.A. and Ferguson, A.J., 2020. Solar thermoradiative-photovoltaic energy conversion. *Cell Reports Physical Science*, 1(12), DOI: 10.1016/j.xcrp.2020.100258.

[21] Ali, H.M., Reda, S.M., Ali, A.I. and Mousa, M.A., 2021. A quick peek at solar cells and a closer insight at perovskite solar cells. *Egyptian Journal of Petroleum*, 30(4), 53-63.

[22] Segev, G., Dotan, H., Ellis, D.S., Piekner, Y., Klotz, D., Beeman, J.W., Cooper, J.K., Grave, D.A., Sharp, I.D. and Rothschild, A., 2018. The spatial collection efficiency of charge carriers in photovoltaic and photoelectrochemical cells. *Joule*, 2(2), 210-224.

[23] Ikegami, T., Maezono, T., Nakanishi, F., Yamagata, Y. and Ebihara, K., 2001. Estimation of equivalent circuit parameters of PV module and its application to optimal operation of PV system. *Solar Energy Materials and Solar Cells*, 67(1-4), 389-395.

[24] El-Ahmar, M.H., El-Sayed, A-H.M. and Hemeida, A.M., 2016. Mathematical modeling of a photovoltaic module and evaluting the effects of various paramenters on its performance. *Proceedings of the 18th International Middle East Power Systems Conference (MEPCON 2016),* Cairo, Egypt, December 27-29, 2016, pp. 741-746.

[25] Singh, B.P. and Singh, R., 2009. Special two-terminal devices. In: D. Kindersley, ed. *Electronic Devices and Integrated Circuits*. Chennai: Pearson Education, pp.880-881.

[26] Sarbu, I. and Sebarchievici, C., 2017. Solar electric cooling systems. In: R. Lisa and C. Maria, eds. *Solar Heating and Cooling Systems*. London: Elsevier, pp. 316-317.

[27] Hassaine, L. and Bengourina, M.R., 2020. Control technique for single phase inverter photovoltaic system connected to the grid. *Energy Reports*, 6(3), 200-208.

[28] Arafa, O.M., Mansour, A.A., Sakkoury, K.S., Atia, Y.A. and Salem, M.M., 2017. Realization of single-phase single-stage grid-connected PV system. *Journal of Electrical Systems and Information Technology*, 4(1), 1-9, DOI: 10.1016/j.jesit.2016.08.004.

[29] Gawhade, P. and Ojha, A., 2021. Recent advances in synchronization techniques for grid-tied PV system: A review. *Energy Reports*, 7, 6581-6599.

[30] Jana, J., Saha, H. and Bhattacharya, K.D., 2017. A review of inverter topologies for single-phase grid-connected photovoltaic systems. *Renewable and Sustainable Energy Reviews*, 72, 1256-1270.

[31] Boulouiha, H.M., Allali, A. and Denai, M., 2016. Grid-integration of wind energy systems: Control design, stability, and power quality issues. In: M.G. Rasul, A.k. Azad and S.C. Sharma, eds. *Clean Energy for Sustainable Development : Comparisons and Contrasts of New Approaches*. Cambridge: Academic Press, pp. 239-335.

[32] Ahmad, I., Fandi, G., Muller, Z. and Tlusty, J., 2019. Voltage quality and power factor improvement in smart grids using controlled DG units. *Energies*, 12(18), DOI: 10.3390/en12183433.

[33] Elkholy, A., Fahmy, F.H., Abou El-Ela, A.A., Nafeh, A.E. and Spea, S.R., 2016. Experimental evaluation of 8 kW grid-connected photovoltaicsystem in Egypt. *Journal of Electrical Systems and Information Technology*, 3(2), 217-229.

[34] Islam, Md.R., Guo, Y. and Zhu, J., 2014. *Power Converters for Medium Voltage Networks*. New York: Springer.

[35] Leung, C.M., Zhuang, X., Friedrichs, D., Li, J., Erickson, R.W., Laletin, V., Popov, M., Srinivasan, G. and Viehland, D., 2017. Highly efficient solid state magnetoelectric gyrators. *Applied Physics Letters*, 111(12), DOI: 10.1063/1.4996242.

[36] Tamilarasi, D. and Sivakumaran, T.S., 2016. Analysis of symmetrical and asymmetrical current source multilevel inverter. *Circuits and Systems*, 7(11), 3469-3484.